Deep Recursive Embedding for High-Dimensional Data

Zixia Zhou, Yuanyuan Wang, *Senior Member*, Boudewijn P.F. Lelieveldt and Qian Tao

Abstract—t-distributed stochastic neighbor embedding (t-SNE) is a well-established visualization method for complex high-dimensional data. However, the original t-SNE method is nonparametric, stochastic, and often cannot well prevserve the global structure of data as it emphasizes local neighborhood. With t-SNE as a reference, we propose to combine the deep neural network (DNN) with the mathematical-grounded embedding rules for high-dimensional data embedding. We first introduce a deep embedding network (DEN) framework, which can learn a parametric mapping from high-dimensional space to low-dimensional embedding. DEN has a flexible architecture that can accommodate different input data (vector, image, or tensor) and loss functions. To improve the embedding performance, a recursive training strategy is proposed to make use of the latent representations extracted by DEN. Finally, we propose a two-stage loss function combining the advantages of two popular embedding methods, namely, t-SNE and uniform manifold approximation and projection (UMAP), for optimal visualization effect. We name the proposed method Deep Recursive Embedding (DRE), which optimizes DEN with a recursive training strategy and two-stage losse. Our experiments demonstrated the excellent performance of the proposed DRE method on high-dimensional data embedding, across a variety of public databases. Remarkably, our comparative results suggested that our proposed DRE could lead to improved global structure preservation.

Index Terms—t-distributed stochastic neighbor embedding, Uniform manifold approximation and projection, deep embedding network, deep recursive embedding, two-stage loss

1 Introduction

Embedding high-dimensional data onto a low-dimensional manifold is of both theoretical and practical value. It can be used for many applications such as data visualization, representation learning, unsupervised clustering, and data exploration [1]-[4]. In recent decades, many dimensional reduction (DR) methods have been proposed. t-distributed stochastic neighbor embedding (t-SNE) [5] is the among most well-known and widely-used methods for high-dimensional data visualization, which preserves local similarity of high-dimensional data in a drastically reduced low-dimensional space (typically 2 for visualization). Nonetheless, there are several issues of t-SNE that may limit its application scenarios. First, t-SNE is stochastic and requires optimization each time, which does not immediately allow out-of-sample projection. Second, the optimization process of the original t-SNE is memory- and time-consuming, not well scalable for large datasets. Third, t-SNE focuses on local neighborhood, often unable to preserve the global data structure well.

To address these issues of t-SNE, a number pf visualization/DR algorithms were proposed after the intial paper of t-SNE. For instance, Barnes-Hut-SNE (BH-SNE) [6], A-tSNE [7] and FIt-SNE [8] were proposed, which can accelerate the computation and reduce memory usage of t-SNE. Lately, the uniform manifold approximation and projection (UMAP) method [9] was introduced, which demonstrated comparable visualization performance as t-SNE but with notably reduced runtime.

In recent years, deep learning techniques have attracted substantial attention in computer vision and machine learning. As a typical example, the auto-encoder (AE) can be seen as a DR method, which embeds high-dimensional data through a deep neural network (DNN). The AE, which aims to reconstruct the original data through an information bottleneck, can extract low-dimensional representation from high-dimensional data, even with the simple minimum square error (MSE) loss function and conventional optimization method [10]. Its embedding performance, however, is generally inferior to that of t-SNE. Nevertheless, AE suggests the great potential of DNN for DR by unsupervised learning.

We hypothesize that the combination of DNN and dedicated, mathematical-grounded DR rules (e.g. entropy, divergence) may further enrich the possibilities and improve the performance of DR. In general, there are two methodologies to combine DNN and DR rules. First, we can enforce the DNN to learn from a standard referenced DR method. Some recent work on deep learning DR follows this rationale, which first calculates a t-SNE or UMAP embedding in standard ways; then trains the DNN to learn t-SNE or UMAP mapping by minimizing the MSE difference [11]. Although this type of methods can achieve scalability and out-of-sample support, their visualization quality has an upper limit equal to that of the referenced method, and

- *Z. Zhou is with the Department of Electronic Engineering, Fudan University, Shanghai 200433, China. E-mail: 16110720022@fudan.edu.cn.*
- *Y. Wang is with the Department of Electronic Engineering, Fudan University, Shanghai 200433, China and Key Laboratory of Medical Imaging Computing and Computer Assisted Intervention of Shanghai, Shanghai 200032, China. E-mail: yywang@fudan.edu.cn.*
- *Boudewijn P.F. Lelieveldt is with the Division of Image Processing, Department of Radiology, Leiden University Medical Center, Albinusdreef 2, 2333 ZA Leiden, the Netherlands. E-mail: B.P.F.Lelieveldt@lumc.nl.*
- *Qian Tao is with the Division of Image Processing, Department of Radiology, Leiden University Medical Center, Albinusdreef 2, 2333 ZA Leiden, the Netherlands. E-mail: q.tao@lumc.nl.*

the network is poor in explainability and generalizability. The second methodology is to train a DNN with dedicated loss functions that capture the mathematical principles of DR. The parametric t-SNE (ptSNE) proposed in 2009 [12] is a pioneering work in this direction, which employed the t-SNE cost function to train a restricted Boltzmann machine (RBM). ptSNE overcomes the stochasticity and unscalability issues of the original t-SNE, but still has a few practical limitations: 1) ptSNE involves a pre-training step and a fine-tuning step, which are complicated to tune while not guaranteed to converge; 2) it adopted t-SNE as its loss function, which indicates that it cannot exceed the performance of the original t-SNE, even if the training converges. Similar to t-SNE, it still emphasized the local structures of data and may not well preserve the global structure.

We seek to develop a parametric (i.e. able to embed new data points) and scalable (i.e. able to embed nearly infinite data points) DR method that can find an intrinsic low-dimensional representation of data, balancing local and global structures. In this paper, we propose a generic deep embedding network (DEN) framework that is based on mathematically grounded DR rules while optimized by DNN. In addition, we proposed a recursive training strategy that can make use of latent features extracted by DEN to further improve the performance of DR, called deep recursive embedding (DRE). We also presented a flexible combination of loss function for excellent visualization performance. The proposed DRE method is able to address the current issues of t-SNE, namely, out-of-sample projection, scalability, and global structure preservation.

2 Related Work and Our Contribution

Principal component analysis (PCA) [13] is a classical DR method, which generate low-dimensional presentation by linearly projecting high-dimensional data points onto the first few principal components. However, the 2D embedding of PCA cannot deliver satisfactory visualization when the data is highly nonlinear.

Manifold learning is another category of DR method by finding non-linear manifold within the high-dimensional space. Manifold learning methods include multiple dimensional scaling (MDS) [14], Isomap [15], Locally Linear Embedding (LLE) [16], and stochastic neighbor embedding (SNE) [17]. They usually deliver better visualization compared with PCA on nonlinear data, but have drawbacks including unscalability, low speed, and poor robustness. In 2008, the t-SNE method [5], a variation of SNE, were first proposed, which later became one of the most popular methods in the scientific society for high-dimensional data visualization. Although t-SNE can generate higher quality embedding results over most other manifold learning methods, it shares similar limitations with them, including stochasticity, unscalability, low speed, and poor global structure preservation. With the KL divergence as loss, t-SNE emphasizes the local neighborhood preservation.

Many interesting developments followed up the original t-SNE [18], [19]. An important work is the Barnes-Hut t-SNE (BH t-SNE) [6], which approximates the high-dimensional space with sparse distributions and uses the Barnes-Hut algorithm to approximate the low-dimensional space. The approximation largely reduces the algorithm complexity and memory consumption, enabling t-SNE to embed very large dataset. Pezzotti et al. proposed a hierarchical stochastic neighbor embedding (HSNE) method to interactively render the visualization at different levels [20]. The hierarchical way of visualization allows small memory footprint by focusing on data landmarks (centroids) instead of all data. The same authors also presented an A-tSNE method [7], which trades off speed and accuracy, to enable interactive data exploration. More recently, Linderman et al. proposed a fast Fourier transform-accelerated interpolation-based t-SNE (FIt-SNE) [8] to significantly accelerate the implementation of t-SNE. Another important embedding method UMAP is introduced in 2018 [9]. The graph-based UMAP is considered competitive with t-SNE in visualization performance and becomes another popular visualization tool. Compared with t-SNE, UMAP is also faster and better scalable. However, it is reported that the performance of UMAP may suffer from the choice of complex hyper-parameters and is sensitive to small data changes [11]. Besides, although some work argues that the global data structure can be better preserved by UMAP, other studies suggested that UMAP preserves the global structure no better than t-SNE when the same initialization was used [21].

With the development of deep learning techniques, a number of recent studies explored DNN for DR. AE is a classical DNN-based DR method, which maps the data to a low-dimensional representation with an encoder and then reconstructs it back to the original dimension with a decoder. Through an unsupervised learning process, the encoder can generate a nonlinear embedding in the low-dimensional representation space. The ptSNE method [12], proposed by van der Maaten in 2009, was based on an early incarnation of DNN. In his work, RBM was used, consisting of three stages: training RBMs, stacking the RBMs to construct a pre-trained NN, and finetuning the pretrained NN. The ptSNE is a parametric way of realizing t-SNE through unsupervised learning. However, its training process is complicated and it is often hard to match the performance of standard t-SNE due to the difficulty of optimization. Another unsupervised method was later proposed to directly cluster data, using a loss function similar to that of t-SNE, but based on estimated centroids [22]. Very recently, another method called DL Projection [11] was introduced to mimic any referenced DR technique: it first selects a front-end method (e.g. t-SNE, UMAP) to generate a projection of a subset; then trains a DNN to learn the referenced embedding. It is simple and intuitive, but there are a few concerns practically and theoretically. First, the performance of the DL projection method is strictly restricted by its front-end t-SNE or UMAP methods, including the embedding quality, scalability and runtime. Second, although the network itself do not demand complex parameter settings, the front-end process still needs elaborate tuning. Third, the method lacks theoretical ground as it performs superficial learning (e.g. minimizes the MSE loss) and

therefore poorly explainable and generalizable.

In brief, we believe DNN methods have great potential for the high-dimensional data embedding task: it is parametric, thereby able to project out-of-sample data, and it is scalable to large input size with the mini-batch strategy. However, most existing DNN-based DR methods are not specialized for the embedding task (e.g. the AE that reconstructs the data using the generic MSE criterion) therefore not competitive in embedding performance. When learning from dedicated DR methods (e.g. the DL Projection method), the performance is still limited to the original referenced DR methods. We believe that the strong feature extraction capability of DNN is under-exploited so far for DR. Latent representations within DNNs can provide rich while concentrated information over the original data, potentially more easily and better embedded in a low-dimensional space. In this work, we propose a novel, dedicated DNN-based DR framework, named *deep embedding network (DEN)*, to embed high-dimensional data in an unsupervised manner. Within this framework, we proposed a *deep recursive embedding (DRE)* method that can make use of the latent representations of the original data for better DR performance.To demonstrate the flexibility of our framework and training strategy, we proposed a *two-stage loss function*, which is able to combine the favorable properties of t-SNE and UMAP.

Specifically, the advantages of the proposed DRE method are five-fold: (1) Like ptSNE, it learns a parametric mapping from high-dimensional space to low-dimensional space, which means any out-of-sample data point can be easily mapped. (2) With mini-batches used for training, the memory consumption and unscalability problems related to $O(N^2)$ are taken care of, where N is the number of data points. No matter how many data points need to be embedded, the memory usage is only related to the fixed batch size, and the computation time is roughly linearly proportional to N, with a complexity of $O(N)$. (3) Compared to ptSNE, the method is more user-friendly to general practitioners of DR, as the DEN architecture is easy to design and to train, without pretraining or fine-tuning. (4) Importantly, we proposed a novel recursive training strategy that can further improve the embedding performance and better preserve global data structure. (5) Finally, we introduced a two-stage loss function, which is able to combine the advantages of t-SNE and UMAP for an optimal visual effect.

3 Methods

3.1 Method overview

The proposed DEN is flexible in its design: it can take in tensors of different dimensions (i.e. not only vector but also tensors). In general, DEN consists of a feature extraction part and a dimension reduction part. With a dedicated embedding loss, the embedding from the high-dimensional data space to the low-dimensional space can be learned.

3.2 Generic DEN Architectures

We present two DEN architectures, hereafter named as Model A and Model B, for vector and image input, respectively. Model A and B are two examples showing that DEN can be very flexible in its design. The introduction of CNN modules in Model B allows extraction of image features tailored to image input, and is extendable to higher-order tensors (e.g. volume). Detailed network architectures of Model A and Model B are shown in Fig. 1.

Each network consists of two parts:

(1) Feature extraction part: In this part, we strive to capture the high-level features with as few layers as possible, to reduce the number of parameters and running time. In our experiments, we determined empirically the parameters of NN (details will be presented in Experiments); however, we note that DEN is very flexible in its architecture design and that the final performance is rather robust to the setting of NN parameters (as will also be shown in Experiments). In Model A, the vector feature extractor contains 5 hidden layers, each of which followed by a ReLU and a batch normalization layer. The batch normalization layers can normalize different batches of data to the same distribution, avoiding gradient vanishing or explosion. In Model B, the first 2 convolutional layers (filter number=16) with ReLU and maxpooling can capture shallow image features, then 2 convolutional layers with 32 filters followed by ReLU and maxpooling operation are used to further extract the features. Afterwards, the feature maps are fed to a convolutional layer with 64 filters for high-level features extraction.

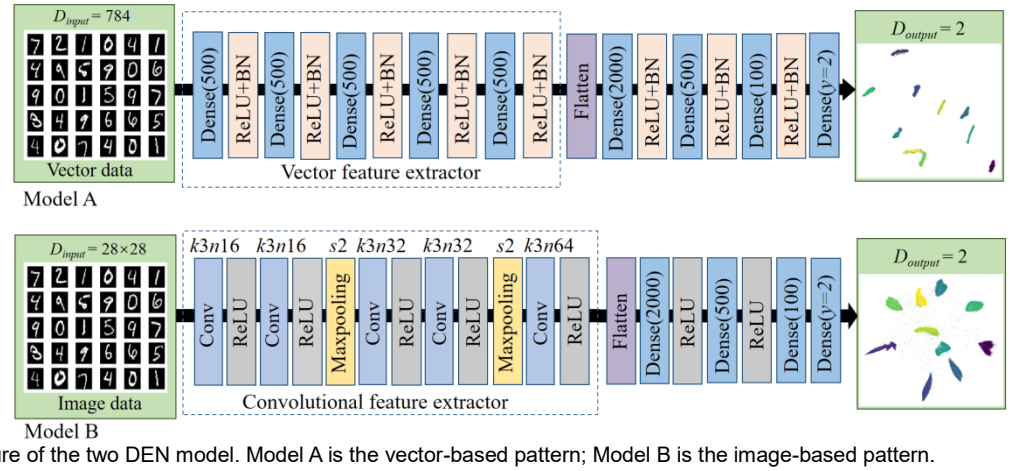

Fig. 1. Architecture of the two DEN model. Model A is the vector-based pattern; Model B is the image-based pattern.

(2) Dimension reduction part: In this part, the dimension is gradually reduced, from 2000 to 500, and then 100, and finally to the target dimension 2. The first dense layer with 2000 neurons is applied to increase the width of the neural network so that its capability to express nonlinear features can be enlarged. Then 2 dense layers with 500 and 100 neurons are used to reduce the dimension, as is often adopted in the design of NN, i.e. a decreasing number of neurons at deeper layers. The setting was empirically chosen, and will be validated in the Experiment section. We will show that the final DR results are not sensitive to the design of the NN, as modern NNs are often robust in optimizing complex cost functions.

3.3 Deep t-SNE and Deep UMAP

With the generic two-part DEN architectures, we formulate dedicated loss functions to guide the training. DEN can take flexible loss functions, including that of t-SNE and UMAP, the two well-established ones. By designing the loss function to represent that of t-SNE or UMAP, we can learn the embedding by DEN parametrically, in an unsupervised manner.

Generally speaking, DEN is optimized by minimizing the difference between the similarity matrices of two-point sets i and j in the high-dimensional and low-dimensional space.

t-SNE [5] minimizes the KL divergence between two probability distributions, P and Q, where P is for x in the high-dimensional space, and Q for their representation y in the low-dimensional space:

$$L_{t-SNE} = KL(P||Q) = \sum_{i \neq j} log \frac{p_{ij}}{q_{ji}} \quad (1)$$

where p_{ij} and q_{ij} are normalized pairwise similarities: p_{ij} is the probability that a data point would choose the data point x_j as its neighbor under the Gaussian distribution in the high-dimensional space, q_{ij} is the probability that a data point y_i would choose the data point y_j as its neighbor under the t-distribution in the low-dimensional space. p_{ij} and q_{ij} are calculated as follows:

$$p_{j|i} = \frac{\exp(-\|x_i - x_j\|^2 / 2\sigma_i^2)}{\sum_{k \neq i} \exp(-\|x_i - x_k\|^2 / 2\sigma_i^2)} \quad (2)$$

$$p_{ij} = \frac{P_{j|i} + P_{i|j}}{2n} \quad (3)$$

$$q_{ij} = \frac{(1 + \|x_i - x_j\|^2 / \sigma)^{\frac{-\alpha-1}{2}}}{\sum_{k \neq i} (1 + \|x_i - x_j\|^2 / \sigma)^{\frac{-\alpha-1}{2}}} \quad (4)$$

where N is the number of data points, σ is the Gaussian kernel, and the degree of freedom of t-distribution α.

UMAP [6] minimizes the cross entropy between two similarity matrices, V and W, where V is for x in the high-dimensional space, and W for their representation y in the low-dimensional space:

$$L_{UMAP} = CE(V||W) = \sum_{i \neq j} v_{ij} log \frac{v_{ij}}{w_{ji}} + (1 - v_{ij}) \log \frac{1 - v_{ij}}{1 - w_{ji}} \quad (5)$$

v_{ij} is calculated as follows:

$$v_{j|i} = \exp[-d(x_i, x_j) - \rho_i / \sigma_i)] \quad (6)$$

$$v_{ij} = (v_{j|i} + v_{i|j}) - v_{j|i} v_{i|ij} \quad (7)$$

where $v_{j|i}$ is calculate only for k approximate nearest neighbors. $d(x_i, x_j)$ is the distance between data point x_i and x_j. ρ_i is the minimum distance between xi and its neighbor. σ_i is defined as follows:

$$\sum_{j=1}^{k} \exp\left(\frac{-\max(0, d(x_i, x_j) - \rho_i)}{\sigma_i}\right) = \log_2(k) \quad (8)$$

Besides, w_{ij} is calculated as:

$$w_{ij} = (1 + a\|y_i - y_j\|_2^{2b})^{-1} \quad (9)$$

where a and b are selected by non-linear least square fitting of

$$\Psi(x, y) \begin{cases} 1 & if \ \|y_i - y_j\|_2 \leq d_{min} \\ \exp(-(\|y_i - y_j\|_2 - d_{min})) & otherwise \end{cases} \quad (10)$$

where $d_{min}$is the desired separation between close points in the embedding space.

We name the DEN trained with the t-SNE and UMAP loss *deep t-SNE* and *deep UMAP*, respectively. In the training process, the mini-batch strategy is used to reduce memory consumption and save running time. We first randomly shuffle the entire dataset, then divide the dataset into mini-batches of a fixed size. After that, the batch are trained one-by-one. When all batches of the entire dataset have been trained once, one epoch is finished. The loss function calculation is similar to the conventional t-SNE and UMAP, and the two probability distributions P and Q are calculated from data within a mini-batch. Take deep t-SNE applied to the MNIST dataset for example, suppose batch size=n, all training images of MNIST datasets (containing 60000 images with size 28*28=784) are divided into $60000/n$ batches. L_{t-SNE} calculates the KL divergence between two probability distributions P and Q, where $P \in \mathbb{R}^{n \times n}$ is calculated from each mini-batch of original high-dimensional data x, $Q \in \mathbb{R}^{n \times n}$ is calculated from the embedded output y. In this case, the network is trained $60000/n$ iterations to finish an epoch, and this process is repeated until the loss converges. The training process of deep UMAP is similar to deep t-SNE: we just need to calculate the batch-wise cross entropy of $V \in \mathbb{R}^{n \times n}$ and $W \in \mathbb{R}^{n \times n}$ as expressed in Eq. (5)-(10) instead of KL divergence of P and Q.

3.4 Deep Recursive Embedding

With introduction of the modern network components, we can largely improve the efficiency and ease of training in Deep t-SNE and Deep UMAP, compared with the RBM-based ptSNE. Nevertheless, the upper limit of the embedding performance remains the same as that of the original t-SNE or UMAP, given that the loss function is based on the original definition. Hence, we further present a recursive training strategy combined with a two-stage loss. Throughout this paper, the Deep t-SNE improved by the recursive training strategy is called the *DR t-SNE* method. The DR t-SNE optimized with the two-stage loss function is called as the *deep recursive embedding (DRE)* method. The schematics of DR t-SNE and DRE is illustrated in Fig. 2.

The recursive training strategy is proposed to make full

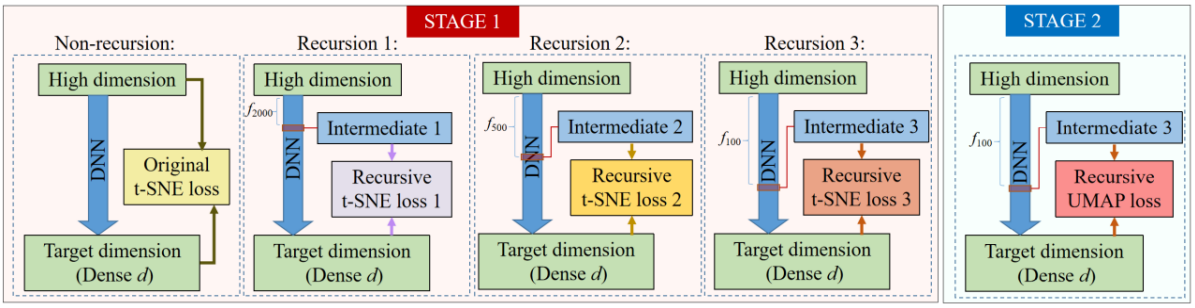

Fig. 2. The schematic of DRE.

use of the rich information from the high-level representations extracted by DEN. The intermediate feature maps extracted from different layers reflect different abstraction levels when solving a specific task. As mentioned in [25] [26], the deeper feature maps of DNN provide more abstract features with inherent data characteristic. For instance, in [27], the authors demonstrated that the deep layers of DNNs can extract a rather rich set of features. Leveraging these intermediate representations for knowledge distillation led to significant improvement in efficiency. In [28], the high-level intermediate feature maps extracted from a pretrained DNN are also adopted as a perceptual loss to improve the image reconstruction performance.

Inspired by such observation, we look into the deep layers of DEN for improved data embedding. In our DRE method, we propose to recursively use the intermediate output of DEN, which represents high-level features of the original input, to embed the original high-dimensional data. This process is called recursive training, as illustrated in Fig. 2. As the lower layers of DEN contain low-level features while the higher layers of DEN extract complex high-level features, we invoke intermediate outputs after the feature extraction path to capture the high-level features at different depths. With high-level feature representation of the original data, we calculate the recursive t-SNE loss and recursive UMAP loss to further optimize the DEN:

$$L'_{t-SNE} = KL(\tilde{P}||Q) \tag{11}$$

$$L'_{UMAP} = CE(\tilde{V}||W) \tag{12}$$

where $\tilde{p}_{j|i}$ and $v_{j|i}$ for $\tilde{P}$ and $\tilde{V}$ are calculated as:

$$\tilde{p}_{j|i} = \frac{\exp(-\|f(x_i)-f(x_j)\|^2/2\sigma_i^2)}{\sum_{k\neq i}\exp(-\|f(x_i)-f(x_k)\|^2/2\sigma_i^2)} \tag{13}$$

$$v_{j|i} = \exp[-d\big(f(x_i), f(x_j)\big) - \rho_i/\sigma_i)] \tag{14}$$

where $f(\cdot)$ is high-level feature extraction function realized by the feature extraction part of DEN.

3.5 Two-Stage Loss

Our design allows flexible combination of the loss function at different stage of recursion. In general, we observed that the UMAP loss can better push the dispersed points between different clusters to their nearest categories (e.g. the UMAP visualization of MNIST), resulting in a desirable visual effect with clean margins between classes (while not necessarily a better classification performance; detailed discussion will be given in Section V-A). This motivated us to introduce a two-stage DRE training strategy: first optimize DEN by the t-SNE loss in a recursive manner, then refine the final visualization by the UMAP loss. The workflow of the proposed DRE is as follows:

In stage 1, the network is first trained using the original t-SNE loss L_{t-SNE} between y and x; then, the network is recursively updated by minimizing the recursive t-SNE loss L'_{t-SNE} between y and the high-level representations intermediately generated by the output of Dense 2000, Dense 500 and Dense 100 layers, where the feature extractors are defined as $f_{2000}(\cdot)$, $f_{500}(\cdot)$, and $f_{100}(\cdot)$, respectively, as shown in the Recursion 1, Recursion 2 and Recursion 3 sections of Fig. 2.

In stage 2, the DEN is further tuned with the UMAP loss to push the dispersed points between different clusters to their nearest categories. This step is optional and largely for visualization purpose.

4 Experiment

4.1 Datasets and Implementation

We experimented with 5 public datasets, covering different data types, sizes, and characteristics: (1) *MNIST* [27], the handwritten digits dataset widely used to evaluate machine learning algorithms, which contains 60000 training images and 10000 testing images with size 28×28, in 10 classes from digit 0 to digit 9. (2) *FashionMNIST* [28], the fashion product database by Zalando, developed in the same format as MNIST, containing 60,000 training images and 10,000 testing images of size 28×28, including 10 classes: T-shirt, trousers, pullover, dress, coat, sandal, shirt, sneaker, bag, and ankle boot. Fashion-MNIST is another benchmark database for machine learning algorithms, more challenging than MNIST. (3) *RNA-Seq* dataset includes 23,822 single-cell transcriptomes. The cells were isolated from the VISp and ALM of adult mouse, coloured by their cluster labels. The cluster label is defined in [29], which is used for visualization. (4) *IMDB* dataset [30] includes 25000 movie ratings data used for sentiment analysis. All data are classified into positive and negative comments. Each data was preprocessed to transform the textual sequences into 500-dimesional word-vectors. (5) *InfiMNIST* [31]: an open source method (Simard et al., 1992) to generate an infinitely large database of handwritten digits based on MNIST. It can be used to test the scalability of

DR algorithms.

Our environment is a Linux workstation with a NVIDIA Tesla V100 GPU, with 50GB system memory and 16GB GPU memory. The network was developed using the Keras library based on the Tensorflow framework [32].

The proposed DEN has a number of hyperparameters, divided into loss-related hyperparameters and network-related hyperparameters. For the loss-related hyperparameters, we set the perplexity to 30 and the degree of freedom of t-distribution to dim-1 = 1 (dim represents the target dimension). For the network-related hyperparameters, a batch size of 2500 is chosen. The Adam optimizer was used for training, with an initial learning rate of 10-3, a β_1 (the exponential decay rate for the 1st moment estimates) of 0.9, a β_2 (the exponential decay rate for the 2st moment estimates) of 0.999 and an epsilon of 10^{-7}. The Deep t-SNE and Deep UMAP were trained 100 epochs. The DR t-SNE has the first 100 epochs trained with the original t-SNE loss, and 50 epochs for each subsequent recursion in Stage 1. In Stage 2, an additional 50 epochs were trained with the UMAP loss.

4.2 Evaluation Metrics

In this work, we used six metrics to evaluate the DR performance [33], [34], namely, 1-nearest neighbor (1NN), neighborhood hit, trustworthiness, continuity, spearman goodness, and normalized stress. The metrics were calculated for the proposed Deep t-SNE, Deep UMAP, DRE with two-stage loss, and the state-of-the-art reference methods. To demonstrate the value of convolution in DEN for image input, we differentiated vector-based deep t-SNE (i.e. flatten the image as a vector) and image-based deep tSNE (i.e. directly use the original image).

1) The 1-nearest neighbor (1NN) classification accuracy is a standard measurement as reported in [5], [12], which can be used to estimate the accuracy of clustering. With its absolute simplicity, the classification accuracy can be an indication of the goodness of clustering in the low-dimensional space.

2) The neighborhood hit measures how well separable the data is in the low-dimensional space, which helps gauge if a technique is good for data exploration. The neighborhood hit is defined as:

$$\sum_{i=1}^{N} \frac{j \epsilon N_i^{(K)} : l_j = l_i}{KN}, \tag{15}$$

which indicates the proportion of the K (K=7 as commonly used in literature) neighbors $N_i^{(K)}$ of a point i in the low-dimensional space that have the same label l as point i itself, averaged over all points in the low-dimensional space.

3) The trustworthiness measures the proportion of points in D that are also close in $P(D)$, which reflects the false neighbors, and tells how much one can trust the local patterns in a projection. The trustworthiness is defined as:

$$1 - \frac{2}{NK(2n-3K-1)} \sum_{i=1}^{N} \sum_{j \epsilon U_i^{(K)}} (r(i,j) - K), \tag{16}$$

where $r(i, j)$ represents the rank of the low-dimensional data point j according to the pairwise distances between the low-dimensional data points, and $U_i^{(K)}$ represents the set of points that are among the K nearest neighbors in the low-dimensional space but not in the high-dimensional space (K=7 as commonly used in literature).

4) The continuity measures the proportion of points in $P(D)$ that are also close together in D, which is closely related to the missing neighbors of a projected point. The continuity is defined as:

$$1 - \frac{2}{NK(2n-3K-1)} \sum_{i=1}^{N} \sum_{j \epsilon V_i^{(K)}} (\hat{r}(i,j) - K), \tag{17}$$

where $\hat{r}(i, j)$ represents the rank of the high dimensional data point j according to the pairwise distances between the low-dimensional data points, and $V_i^{(K)}$ represents the set of points that are among the K nearest neighbors in the high-dimensional space but not in the low-dimensional space (K=7 as commonly used in literature).

5) The normalized stress measures the preservation of point-pairwise distances, which can be expressed as:

$$\frac{\sum_{i,j} \left(\Delta^n(x_i,x_j) - \Delta^q(P(x_i),P(x_j))\right)^2}{\sum_{i,j} \Delta^n(x_i,x_j)}, \tag{18}$$

where Δ^n and Δ^q are distance metrics for data points in low and high dimensional space, respectively.

6) The Shepard goodness measures the overall distance preservation by computing the Spearman rank correlation of Shepard diagram. The formula of generating a Shepard diagram is defined as:

$$\text{Scatterplot}\left(\|x_i - x_j\|, \|P(x_i) - P(x_j)\|\right), 1 \le i \le N, i \ne j. \tag{19}$$

5 Results

5.1 Evaluation of the Feature Extractor in Different Deep Networks

Our proposed DEN architecture consists of two parts: the feature extraction part and dimensionality reduction part. To explore how the intermediate representations in DEN are distributed in different learning-based methods, we used the BH t-SNE as a visualization tool to check the intermediate 500-dimensional features. We compared deep networks with different structures and loss functions, including (1) the AE with hidden layer setting 784-1000-500-100-2-100-500 (selected intermediate layer) -1000-784, (2) image-based deep UMAP, (3) vector-based deep t-SNE, (4) image-based deep t-SNE, (4) image-based DR UMAP, (5) vector-based DR t-SNE, and (6) image-based DR t-SNE. Here vector-based and image-based refer to Model A and Model B architectures, respectively. All six methods were evaluated on MNIST and fashion-MNIST datasets, as shown in Fig. 5 (a) and (b).

For the MNIST dataset, it can be seen that the AE separate number 5 into two parts, and both deep UMAP and DR UMAP confused 4 and 9 as shown in Fig. 5 (a). Such phenomenon is observed in both the BH t-SNE map of intermediate features as well as in the final embedding. In contrast, the vector-based and image-based deep t-SNE resulted in well separated clusters at the intermediate layer as well as the final embedding. When the proposed recursive training strategy was applied (namely, DR UMAP and DR t-SNE), we observed an even better separation of the clusters, especially the DR t-SNE which showed clear and well-separated clusters. Such results suggest the superior

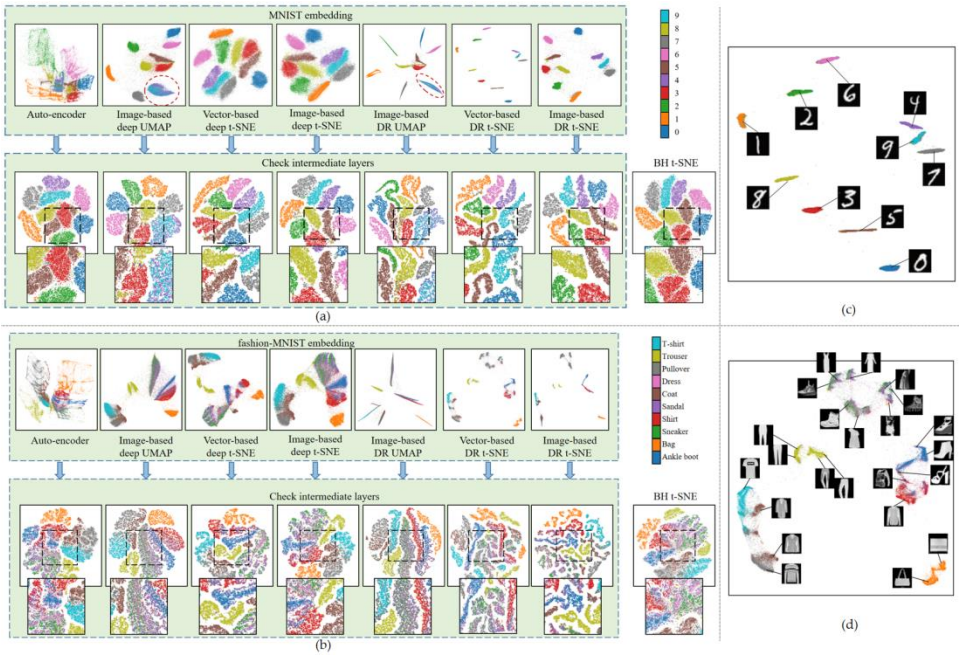

Fig. 5. The first rows of (a) and (b) show the MNIST and fashion-MNIST 2D embeddings by different methods: autoencoder, Deep UMAP, Deep t-SNE, DR UMAP and DR t-SNE, and the second rows of (a) and (b) are BH t-SNE visualizations of the latent features within the deep network (Section 3.1 explains where such features are extracted). (c) and (d) show some sample images of different clusters visualized by DR t-SNE.

intermediate feature extraction capability of the proposed recursive training strategy.

The classes in the fashion-MNIST dataset are traditionally more difficult to separate than MNIST: images within the same category may have certain discrepancies (e.g. dresses), while images from difference categories may bear resemblance to each other (e.g. sandals and sneakers). As shown in Fig. 5 (b), dresses contain a wide variety of styles, some of which can confuse with sneakers. The Deep UMAP tends to group coarse classes but mix the fine classes, while the Deep t-SNE can generate finer classes while maintaining the relative distances of coarse classes. We noticed that this characteristic is more pronounced in the comparison between DR UMAP and DR t-SNE. The recursive training strategy helps the DR UMAP get coarse clusters, while prompts DR t-SNE to obtain fine clusters based on subtle feature. To further examine this characteristic, we display some typical cases of each fine cluster in the image-based DR t-SNE result, as shown in Fig. 5 (c) and (d). Take Fig. 5 (d) for examples, bags are divided into two subclasses based on whether they have carry-handles; trousers are split in two sub-group through their folding manners; dress class has more fine clusters based on their styles (sleeve length, design of the waist/swing, single shoulder and etc.). Such results suggest the global feature extraction capability of the proposed DR t-SNE method.

5.2 Evaluation of Netowrk Settings

In this part of experiments, we evaluated the choice of hyperparameters in our network design, namely, number of layers and neurons in the feature extraction part and dimension reduction part. Fig. 6. (a)-(c) show the results of DR t-SNE (trained by Model A) with 3, 5, and 8 dense layers in the feature extraction part, respectively. The results of three settings show no obvious difference. The result obtained by the DR t-SNE with 5 dense layers shows a slight increase in the 1NN classification accuracy. (d)-(f) are results of DRE (trained by Model B) with 3, 5 and 8 convolutional layers in feature extraction part, respectively. It can be observed that 3 convolutional layers are not adequate to capture the complex features, leading to a separate cluster of number 2. The results of 5 and 8 convolutional layers are similar, while our finally selected setting (5 convolutional layers) shows a minor advantage in the 1NN classification accuracy. (g)-(i) are results of DRE designed as 2000-2, 2000-500-100-2 and 2000-500-100-50-2 in the feature extraction part, respectively. It can be observed that fewer layers

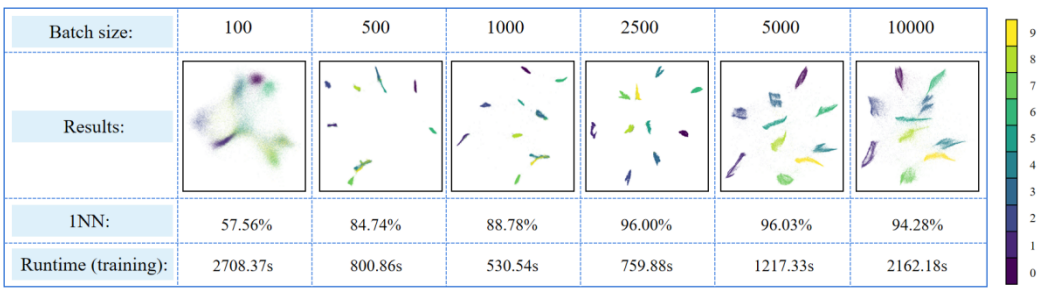

Fig. 7. Comparisons of embedding results obtained by different batch size settings.

tend to generate loose clusters (although good enough for separation), while more layers lead to better distinguishable clusters and slightly better 1NN classification performance. We find 2000-500-100-2 an appropriate choice. (j)-(l) are results of the DR t-SNE trained with different perplexities. As shown, the perplexity only has minor influences on the embedding results, while the 1NN classification accuracy indicates a small advantage of our selected perplexity of 30.

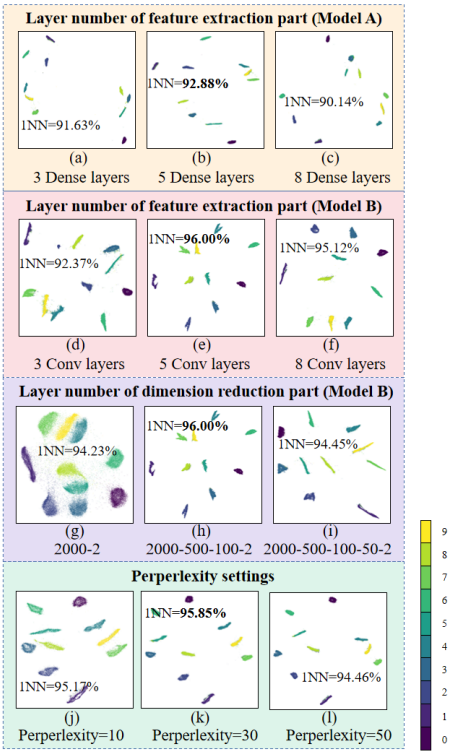

Fig. 6. Comparisons of embedding results obtained by different network settings.

We also evaluated the influence of mini-batch size on the final results. Our experiments showed that the mini-batch size had influence on both visualization and runtime performance. We recorded the DRE results using different mini-batch sizes, as shown in Fig. 7. In terms of visualization performance, the result obtained with batch size=100 had fuzzy clusters. The results obtained with batch size=500 and 1000 showed clearer clusters, but with some classes still close to each other. DRE with batchsize=2500 and 5000 showed improved results, with well-distinguishable clusters. Larger batch size over 10000 led to dispersion within each cluster, as larger batch allows extraction of more detailed information within clusters.

In terms of the runtime performance, DRE with batchsize=1000 is the fastest, as listed in Fig. 7. Smaller batch size leads to more training iterations to reach convergence, while larger batch size results in dramatically increased time and memory consumption for calculating the probability distribution of high dimensional data P_{ij}. Overall, we selected batch size=2500 as an appropriate choice compromising both visualization performance and runtime efficiency.

5.3 Evaluation of Recursive Training Strategy

During recursive training, we observed that the clusters were gradually finetuned to better reflect the inter-cluster relationship, resulting in better separated while denser clusters. Similarly, FIt-SNE demonstrates the same effect with its late exaggeration. To evaluate the difference between FIt-SNE and DRE, we implemented FIt-SNE with different late exaggeration settings, and trained DRE with different number of recursions. As shown in the left panel of Fig. 8, FIt-SNE with different late exaggerations are evaluated on MNIST, Fashion-MNIST RNA-Seq and IMDB da-

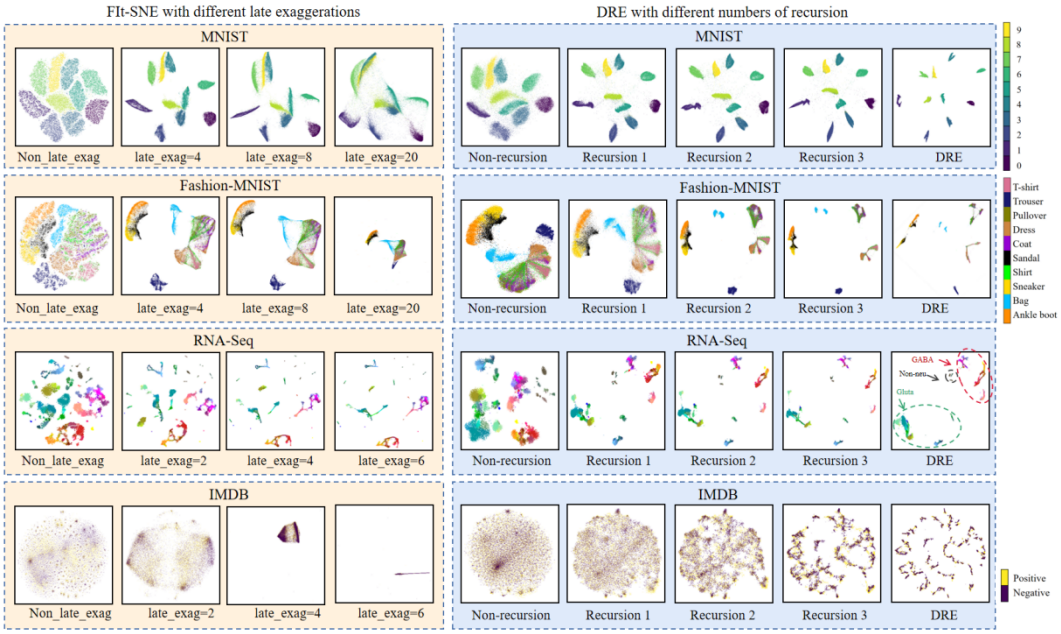

Fig. 8. Embedding performances of FIt-SNE with different late exaggeration settings (left panel) and DRE with different recursions (right panel). For RNA-Seq dataset, cluster colours followed the setting of the original publication [29], where warm colours correspond to inhibitory neurons, cold colours correspond to excitatory neurons, brown/grey colours correspond to non-neural cells.

tasets. Fit-SNE shrinks clusters with increased late exaggeration, but it can hardly alter the overall distribution of clusters. As shown in the right panel of Fig. 8, for the MNIST, fashion-MNIST, RNA-Seq and IMDB datasets, the recursion process reduces the intra-class distances and results in a clearer global overview. In particular, for the RNA-Seq data, the three major cell classes, namely, GABA, Gluta and Non-neu, exhibits long inter-class distances and short intra-class distances, clearly showing the global data structure.

Fig. 9 displays the network loss with and without recursive training strategy. From the network loss, it can be observed that when P (generated from the original high-dimensional data) are replaced by $\tilde{P}$ (generated from the high-level features), the network loss reduces more rapidly than the non-recursion method. This finding implies that the high-level features may contain useful latent information. The rich latent information may help breakthrough the bottleneck of the original t-SNE, which only perform computation on the original data. To make a fair comparison, the t-SNE loss of the original data, i.e. $KL(P||Q)$ instead of $KL(\tilde{P}||Q)$, during the recursive training are also plotted in Fig. 9. It roughly follows the original loss curve but exhibits an accelerated reduction. We note that the loss may not be a surrogate of the visualization performance, as the recursive training results in better embedding with global structure, which can be visually appreciated but may not be reflected in the loss.

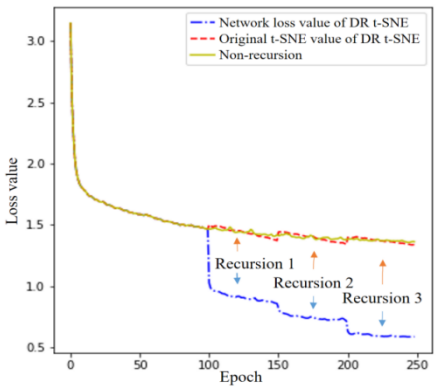

Fig. 9. The training loss of deep t-SNE with/without recursive training strategy.

5.4 Comparison between Different Embedding Methods

We compared the proposed DEN methods with other reference methods on the MNIST, Fashion MNIST, RNA-Seq and IMDB datasets. We compared in total 12 methods for a comprehensive evaluation: (1) PCA, (2) AE, (3) BH t-SNE, (4) FIt-SNE, (5) UMAP, (6) RBM ptSNE, (7) Direct DL Projection trained using t-SNE as reference, (8) Direct DL projection trained using UMAP as reference, (9) Deep t-SNE, (10) vector-based DR t-SNE, (11) image-based DR t-SNE, and (12) DRE with two-stage loss. Fig. 10 shows the results of MNIST and fahison-MNIST 2D embedding, both

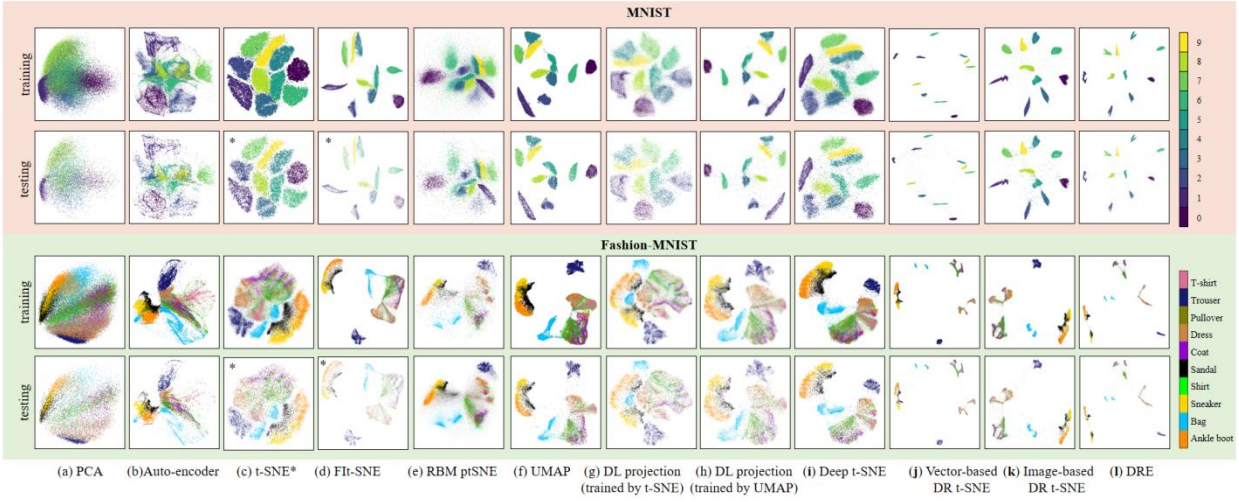

Fig. 10. Comparison of embedding performance on both the MNIST and Fashion-MNIST datasets. * indicates the displayed testing results are embedded in training process because the non-parametric methods cannot perform a testing process.

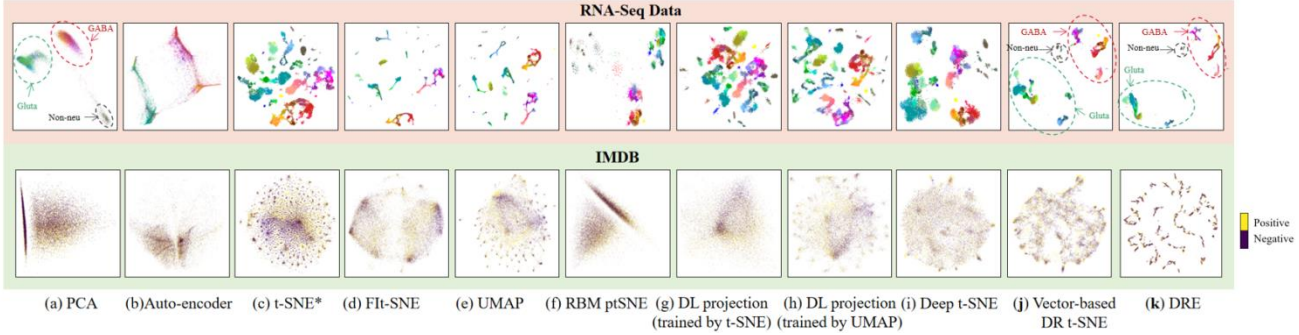

Fig. 11. Comparison of embedding performance on RNA-Seq and IMDB datasets. For RNA-Seq dataset, cluster colours followed the setting of the original publication [29], where warm colours correspond to inhibitory neurons, cold colours correspond to excitatory neurons, brown/grey colours correspond to non-neural cells.

TABLE I

COMPARISON OF THE EMBEDDING PERFORMANCE ON MNIST, FASHION-MNIST, IMDB AND RNA-SEQ DATA, BY DIFFERENT METHODS. M_{NH}, M_t, M_C, M_σ, M_S INDICATE THE VALUES OF NEIGHBORHOOD HIT, TRUSTWORTHINESS, CONTINUITY, SPEARMAN GOODNESS, AND NORMALIZED STRESS, RESPECTIVELY.

Experiments		PCA	Auto-encoder	BH t-SNE	FIt-SNE*	UMAP	RBM ptSNE	DL projections (t-SNE)	DL projections (UMAP)	Deep t-SNE	**DR t-SNE (Vector)**	**DR t-SNE (Image)**	**DRE**
MNIST	1NN (Testing)	38.93%	73.95%			93.25%	84.93%	88.97%	93.12%	89.84%	92.88%	95.85%	96.00%
	1NN (Training)	38.64%	82.43%	96.05%	94.21%	94.45%	86.64%	92.19%	93.59%	93.05%	94.13%	96.07%	96.10%
	M_{NH}	0.47	0.80	0.93	0.92	0.92	0.81	0.90	0.95	0.93	0.93	0.96	0.97
	M_t	0.74	0.94	0.98	0.95	0.96	0.92	0.92	0.93	0.94	0.93	0.94	0.92
	M_C	0.94	0.96	0.98	0.98	0.97	0.97	0.97	0.97	0.97	0.96	0.97	0.96
	1-M_σ	0.42	0.43	0.54	0.54	0.50	0.24	0.53	0.54	0.53	0.52	0.54	0.52
	M_S	0.50	0.43	0.43	0.39	0.37	0.53	0.32	0.31	0.34	0.28	0.29	0.29
Fashion-MNIST	1NN (Testing)	44.87%	64.95%			67.81%	68.01%	67.44%	67.76%	68.27%	67.83%	69.73%	69.08%
	1NN (Training)	44.72%	68.69%	79.85%	71.05%	72.07%	68.90%	69.79%	70.23%	68.35%	68.84%	69.87%	68.94%
	M_{NH}	0.53	0.71	0.77	0.77	0.73	0.70	0.71	0.73	0.73	0.72	0.76	0.77
	M_t	0.91	0.97	0.99	0.99	0.98	0.97	0.96	0.96	0.97	0.97	0.97	0.97
	M_C	0.98	0.98	0.99	0.99	0.99	0.99	0.98	0.99	0.99	0.98	0.98	0.98
	1-M_σ	0.65	0.50	0.61	0.64	0.56	0.63	0.61	0.65	0.62	0.56	0.60	0.62
	M_S	0.88	0.72	0.58	0.65	0.58	0.76	0.50	0.63	0.63	0.53	0.60	0.59
IMDB	M_{NH}	0.59	0.59	0.65	0.62	0.65	0.59	0.61	0.62	0.59	0.67		0.74
	M_t	0.69	0.62	0.89	0.72	0.79	0.68	0.63	0.67	0.72	0.74		0.74
	M_C	0.66	0.63	0.84	0.80	0.85	0.70	0.75	0.76	0.80	0.80		0.79
	1-M_σ	0.26	0.23	0.34	0.38	0.32	0.23	0.24	0.28	0.35	0.41		0.40
	M_S	0.16	0.08	0.29	0.27	0.26	0.37	0.34	0.29	0.41	0.37		0.36
RNA-Seq	M_{NH}	0.91	0.27	0.99	1.00	1.00	0.96	0.98	0.99	1.00	1.00		1.00
	M_t	0.85	0.82	1.00	0.99	0.99	0.98	0.98	0.98	0.99	0.98		0.98
	M_C	0.93	0.91	1.00	1.00	0.99	0.99	0.99	0.98	0.99	0.99		0.99
	1-M_σ	0.53	0.51	0.59	0.62	0.61	0.56	0.55	0.61	0.51	0.51		0.50
	M_S	0.88	0.44	0.40	0.58	0.55	0.79	0.30	0.56	0.59	0.56		0.62

in training and testing. For the conventional t-SNE, we embedded the training and testing data separately as there is no learning mechanism. We also quantitatively evaluated the embedding performance of MNIST and Fashion MNIST data, as reported in Table I.

The results of the MNIST dataset are shown in Fig. 10 and reported in Table I. It can be observed that the PCA method can hardly differentiate the 10 classes, with poor performance in terms of 1NN error and neighborhood hit. The AE performs better than PCA in terms of 1NN error, neighborhood hit, and trustworthiness, but the embedding remains visually confusing. The Barnes-Hut t-SNE and UMAP are the two currently most popular visualization methods, which generate excellent results both in visualization and quantitative assessment in contrast to AE. The FIt-SNE (late exaggeration=6) shows tighter clusters for each class and comparable quantitative performance to that of Barnes-Hut t-SNE. The RBM ptSNE is a parametric realization of standard t-SNE, but the visual results and stress value appear worse than that of BH t-SNE. The proposed Deep t-SNE, which is easier to train than ptSNE, exhibits improved embedding performance over the RBM-based ptSNE. With introduction of the recursive training strategy, the DR t-SNE and DRE (with two-stage loss) both produce visually improved 2D embeddings with clear global data structure. This is in contrast to the Barnes-Hut t-SNE - when applied to the training and testing data separately, the global structure change (not only rotational but also in relative position of clusters). Besides, our proposed DRE method shows superior 1NN and neighborhood hit value, comparable trustworthiness, continuity and normalized stress to those from the t-SNE and UMAP methods. We noticed that the Shepard goodness is reduced compared to the standard methods, as the recursive training strategy exaggerates the inter-cluster distances by utilizing intermediate representations of the original data, while Shepard goodness is a measure based on the original

data.

For the Fashion-MNIST dataset, more distinct clusters (e.g. tops, bottoms and shoes) are shown up by our method. The confusion of certain classes (e.g. shirt, pullover and coat), however, is similar by our methods as by UMAP. Besides, while Fashion-MNIST is generally considered to be more challenging than MNIST, our DRE method exhibited close quantitative measures of embedding performance on Fashion-MNIST and MNIST.

The results of RNA-Seq is shown in the first column of Fig. 11 and Table I. The RNA-Seq can be divided into three major types—glutamatergic (excitatory) neurons (GABA),

TABLE II

COMPARISON OF THE EMBEDDING PERFORMANCE OF THE 1 MILLION INFIMNIST DATA, EMBEDDED BY LEARNING FROM TRAINING DATA OF DIFFERENT SIZE. THE EMBEDDING PERFORMANCE IS QUANTIFIED BY THE 1NN CLASSIFICATION ACCURACY.

Training data size	PCA	Auto- encoder	UMAP	RBM ptSNE	DL projection (t-SNE)	DL projection (UMAP)	Deep t-SNE	Vector-based DR t-SNE	Image-based DR t-SNE	DRE
0.05 million	35.80%	64.14%	87.00%	64.84%	83.68%	86.52%	89.96%	91.12%	93.33%	93.52%
0.1 million	39.14%	68.35%	90.25%	71.14%	87.61%	90.23%	91.64%	92.98%	95.48%	95.58%
0.3 million	52.36%	78.50%	93.60%	82.38%	90.39%	93.07%	94.76%	95.05%	97.14%	97.17%

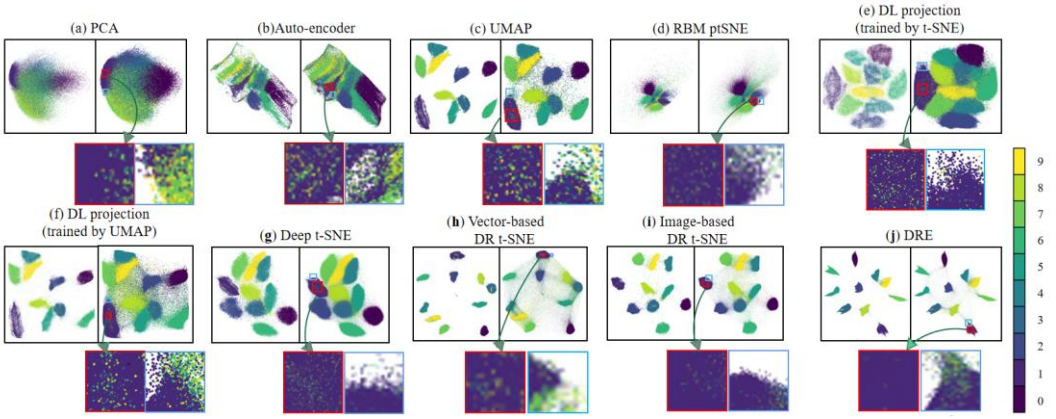

Fig. 12. Embedding 1 million InfiMNIST data by learning from 0.1 million data. The embeddings of both training and testing data are shown for PCA, autoencoder, UMAP, RBM ptSNE, DL projection (trained by t-SNE), DL projection (trained by UMAP), vector-based DR t-SNE, image-based DR t-SNE and DRE method. Local neighborhoods are zoomed in for a closer check.

TABLE III

COMPARISON OF THE EMBEDDING PERFORMANCE OF THE INCREASINGLY LARGE MNIST DATA, EMBEDDED BY LEARNING FROM TRAINING DATA OF 10K. THE EMBEDDING PERFORMANCE IS QUANTIFIED BY THE 1-NEAREST NEIGHBOR CLASSIFICATION ACCURACY.

Testing data size	PCA	Auto- encoder	UMAP	RBM ptSNE	DL projection (t-SNE)	DL projection (UMAP)	Deep t-SNE	Vector-based DR t-SNE	Image-based DR t-SNE	DRE
5K	36.84%	67.06%	87.70%	68.06%	82.14%	84.92%	86.65%	86.56%	89.96%	89.68%
10K	37.32%	67.43%	78.98%	68.58%	82.31%	85.08%	87.09%	85.77%	89.83%	90.07%
30K	37.85%	66.89%	87.76%	67.79%	81.66%	84.45%	87.01%	86.00%	90.09%	90.08%
60K	38.10%	67.47%	88.01%	68.47%	82.06%	84.75%	87.26%	86.62%	90.49%	90.67%

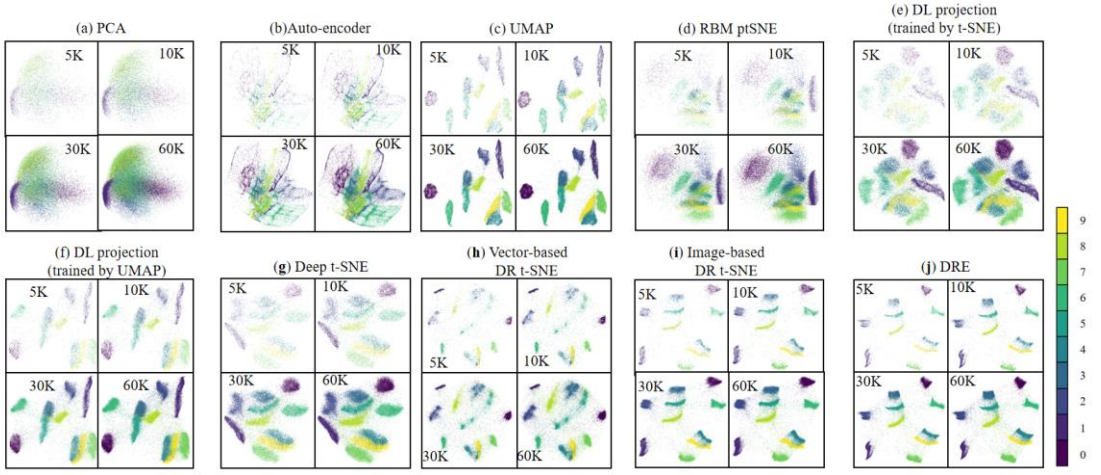

Fig. 13. Embedding increasingly large MNIST data by learning from 10K data. The embeddings of testing data of 5K, 10K, 30K and 60K are shown for PCA, autoencoder, UMAP, RBM ptSNE, DL projection (trained by t-SNE), DL projection (trained by UMAP), vector-based DR t-SNE, image-based DR t-SNE and DRE method.

TABLE IV
COMPARISON OF THE RUNTIME OF DIFFERENT EMBEDDING METHODS (MNIST: 60,000 TRAINING AND 10,000 TESTING)

		Type					Parametric				Non-parametric			
Method		PCA	Auto- encoder	RBM ptSNE	UMAP	Deep t-SNE	DL projection (t-SNE)	DL projection (UMAP)	DR t-SNE	DRE	Eigenmaps	BH t-SNE	Open t-SNE	FIt-SNE
Runtime (second)	Train	0.029	31.78	7455.39	83.88	250.81	2212.01	1085.72	339.51	759.88	42026.70	5730.79	1149.47	304.17
	Test	0.67	0.46	0.49	13.68	0.84	0.22	0.40	0.82	0.73				

GABAergic (inhibitory) neurons (Gluta) and non-neuronal cells (Non-neu). As shown in the first row of Fig. 11, the GABA, Gluta and Non-neu classes are well differentiated by PCA, which preserves the global structure of data. However, the local data structures are highly nonlinear, as shown by the indistinguishable sub-types. The t-SNE, FIt-SNE, UMAP, DL projection and Deep t-SNE methods, in comparison, show good performance of intra-class visualization as they better emphasize local neighborhood. Nevertheless, the global structure of data, as clearly depicted by PCA, is largely lost. In comparison, our proposed DR t-SNE and DRE methods showed improved balance over the standard t-SNE and UMAP methods in that it better preserves both global and local structures of data. The three major types of brain cells are well separated, in resemblance to the PCA result, while sub-types can also be observed within each major type, in a hierarchical manner.

The results of IMDB dataset is shown in the second row of Fig. 11 and Table I. Although the data are only roughly classified into positive and negative comments, the actual sentiments are complex and diverse. We observed that PCA, AE, and RBM ptSNE all embed the IMDB data into two clusters, but cannot reflect more detailed semantic characteristics. The result of FIt-SNE (late exaggeration=2) is similar to those of the PCA, AE and RBM ptSNE, but some blurry sub-clusters can already be observed. The results of t-SNE and UMAP show a number of tight clusters in an umbrella shape, which can hardly reflect the global structure of semantics. In comparison, the results of the proposed DR t-SNE and DRE show a better representation of the rich semantic information (which can potentially be revealed using more semantic labels). Quantitatively, the evaluation metrics also indicate an advantage of our proposed DRE, with the highest neighborhood hit, trustworthiness and spearman goodness, and lowest normalized stress.

5.4 SCALABILITY OF DRE

To evaluate scalability, we generated huge training and testing datasets of InfiMNIST, and evaluated if the proposed deep learning method could embed data on extremely large scale. We trained the proposed method for 2D embedding using 0.05 million, 0.1 million and 0.3 million InfiMNIST dataset, and embedded an independently generated 1 million InfiMNIST testing dataset. Then we measured the 1NN classification accuracy on the 2D embedding, as reported in Table. II. The proposed DRE method outperformed all other embedding methods, with a 93.52%, 95.58% and 97.17% testing accuracy when trained on 0.05 million, 0.1 million and 0.3 million data, respectively. Fig. 12 shows the embedding results of the 1 million testing data (trained on 0.1 million data), for PCA, AE, UMAP, RBM ptSNE, DL projection (t-SNE), DL projection (UMAP), Deep t-SNE, vector-based DR t-SNE, image-based DR t-SNE, and DRE with two-stage loss, respectively. The embedding of both the training (left) and testing (right) datasets are shown. We zoomed in the local neighborhood inside and outside a class. It can be observed that the proposed DR t-SNE produced clean neighborhood both inside and outside the class, which explains the high classification accuracy. (All figures are plotted in the same way, including ordering.) Overall, the DRE method showed the best visual and quantitative performance on embedding a million data points.

In addition, we also used a small training set containing 10K data points to train the embedding methods, and tested them on an increasingly large testing set. The comparison is shown in Fig. 13 and Table IV. It can be observed except for the UMAP method, all other learning-based methods show stable performance. Overall, the image-based DR t-SNE and DRE with two-stage loss showed the best performance among all methods.

5.5 RUNTIME

Runtime of different embedding methods are reported in Table IV. The PCA, Eigenmaps and BH t-SNE methods were implemented single threaded on CPU. UMAP used numba's parallel implementation to do multithreaded processing with multiple cores on CPU. The DL projection methods adopted the MulticoreTSNE with 8 NVIDIA Tesla V100 GPU to parallelly calculate the network references, and fitted the model using only 1 GPU. The Open t-SNE and FIt-SNE utilized the multithreading and C/C++ compiler on CPU. The proposed methods single threaded all computations, and used 1 GPU to train the networks. As shown in Table IV, the runtime of the proposed Deep t-SNE, DR t-SNE and DRE increased gradually due to the multiple recursion. Compared with non-parametric methods, the DRE method needed less runtime than the publicly available Open t-SNE [35], but more runtime than FIt-SNE [8]. Among the parametric methods, the proposed methods were faster than the original RBM-based ptSNE method, but still slower than AE and UMAP.

6 DISCUSSION

In this work, we proposed to combine the modern DNN and mathematically-grounded embedding rules to embed complex, high-dimensional data, and we name this framework as DEN. The generic framework of DEN can be designed in a flexible manner, in terms of architecture, training strategies, and loss function. Based on DEN, we showed how to design Deep t-SNE and Deep UMAP, and further proposed a recursive training strategy for DR t-

SNE and DR UMAP. Finally, we proposed a DRE method, a DEN trained recursively with a two-stage loss including both t-SNE and UMAP.

The proposed DRE has the following advantages compared to the classical t-SNE: (1) the DRE method is learning-based and can easily embed new data; (2) the DRE method is more scalable in speed and memory than t-SNE, able to processing data of extremely large size; (3) the proposed recursive training strategy showed to preserve the global data structure better than t-SNE; (4) DRE used a two-stage loss and can combine the advantages of both t-SNE and UMAP for data embedding and visualization. We carried out extensive experiments and tested DRE on a variety of public datasets. The performance was evaluated both visually and quantitatively using six quality metrics. The DRE method demonstrated excellent performance, in comparison with a collection of classical and state-of-the-art data embedding methods.

We also demonstrated that our proposed DRE method is easy to use. Among its network hyperparameters, the mini-batch size has certain influence on the final results: a small mini-batche cannot fully sample the data distribution, while a big mini-batch may require too large memory to calculate P. Other network settings only had minor influence on the final performance. Therefore, the hyperparameters can be fixed in most cases, making it an easy and generic tool. Another hyperparameter is the number of the recursions, for which we can use a simple rule of thumb: if we are more interested in the global structure of data, we can increase the number of recursions (e.g. 3) and obtain better separated clusters in a global view since the intermediate latent features provide an exaggeration effect; otherwise 1 or 2 recursions are sufficient to visualize the global data structure and local details.

As shown by the experiments in Section 5.4, all parametric embedding methods can map a large, out-of-sample datasets. It is an inherent advantage of learning-based methods. However, the training mechanisms of the presented learning-based methods are very different. The DL projection method is directly learning the DR results, which first calculates a t-SNE or UMAP in conventional ways, and then train a DNN to fit the t-SNE or UMAP embedding results. In contrast, our proposed DEN methods enforce the network to learn the embedding rules (instead of embedding results), e.g. the minimization of KL divergence or the cross-entropy. Both combine DNN with the concepts of t-SNE or UMAP, however, the performance of the DL projection method is restricted by its teacher. This is demonstrated visually and quantitatively in our experiments. In contrast, the better integration of DNN and mathematically-grounded embedding rules by DEN allows (1) faster training as it does not need prior calculation of the reference, (2) better performance as it learns the inherent embedding rules, and (3) systematic improvement as the recursive training strategy can be introduced in an integral manner, taking advantages of the latent representations extracted by DEN.

There are a few practical weaknesses of the proposed DEN methods. First, the proposed methods (deep t-SNE, deep UMAP, DR t-SNE, DR UMAP, DRE) obtain the parametric embedding by learning from a dataset, and are more suitable for big data datasets than for small datasets. Second, the proposed methods still need more runtime than PCA, AE and UMAP. Nevertheless, we expect that the runtime can be reduced by multithreaded calculation of P for different mini-batches.

7 Conclusion

In this paper, we introduced a generic DEN framework, which is flexible in its architecture, training strategies, and loss function. Based on DEN, we proposed a number of variants to embed and visualize the high-dimensional data. The proposed framework can combine the advantages of both t-SNE and UMAP, or any popular embedding methods. The DRE method with recusive training and two-stage loss showed excellent performance in comparison with other state-of-the-art data embedding and visualization methods. DRE is parametric, scalable, easy to implement, and can achieve a good balance between global and local data structure visualization on a wide variety of databases.

References

[1] B. Wang et al., “Visualization and analysis of single-cell RNA-seq data by kernel-based similarity learning,” Nature methods, vol. 14, pp. 414–416, 2017.

[2] Y. Bengio. “Deep learning of representations: Looking forward,” CoRR, abs/1305.0445, 2013.

[3] Y. Bengio et al., “Unsupervised feature learning and deep learning: A review and new perspectives,” CoRR, abs/1206.5538, 2012.

[4] S. Liu et al., “Visualizing high-dimensional data: advances in the past decade,” IEEE Transactions on Visualization and Computer Graphics, vol. 23, pp. 1249–1268, 2017.

[5] L. van der Maaten, and G. Hinton, “Visualizing data using t-SNE. Journal of machine learning research,” pp. 2579-2605, 2008.

[6] L. van der Maaten, “Accelerating t-SNE using tree-based algorithms,” Journal of machine learning research, pp. 3221–3245, 2014.

[7] N. Pezzotti et al., "Approximated and user steerable tSNE for progressive visual analytics," in IEEE Transactions on Visualization and Computer Graphics, vol. 23, no. 7, pp. 1739-1752, 2017.

[8] G. Linderman et al. “Fast interpolation-based t-SNE for improved visualization of single-cell RNA-seq data,” Nature Methods, vol. 16, pp. 243-245, 2019.

[9] L. McInnes and J. Healy, “UMAP: Uniform manifold approximation and projection for dimension reduction,” ArXiv preprints, February 2018.

[10] A. Makhzani et al., “Adversarial autoencoders,” in International Conference on Learning Representations, 2016.

[11] M. Espadoto et al, “Deep learning multidimensional projections”, ArXiv Preprint: DOI: https://doi.org/10.1177/1473871620909485, 2020.

[12] L. van der Maaten, “Learning a parametric embedding by preserving local structure,” in International Conference on Artificial Intelligence and Statistics, vol. 5, pp. 384–391, 2009.

[13] T. I. Jolliffe, “Principal component analysis,” Journal of Marketing Research, vol 87, no, 4, pp. 513, 2002.

[14] A. Buja et al., “Data visualization with multidimensional scaling,” Journal of Computational & Graphical Statistics, vol. 17, vol.2, pp. 444-472,

2008.

[15] M. Balasubramanian and E, L. Schwartz, “The Isomap algorithm and topological stability,” Science, 295(5552):7.

[16] S. Roweis et al. “Nonlinear dimensionality reduction by locally linear embedding. Science, 290(5500): 2323-2326, 2000.

[17] G. E. Hinton and S. T. Roweis, “Stochastic neighbor embedding,” In Advances in Neural Information Processing Systems, pp. 857–864. MIT Press, 2003.

[18] D. Chan et al., “T-SNE-CUDA: GPU-accelerated t-SNE and its applications to modern data,” In 30th International Symposium on Computer Architecture and High Performance Computing (SBAC-PAD), pp. 330–338, Sep. 2018. DOI: 10.1109/CAHPC.2018.8645912

[19] N. Pezzotti et al., "GPGPU Linear complexity t-SNE optimization," IEEE Transactions on Visualization and Computer Graphics, vol. 26, no. 1, 2020.

[20] N. Pezzotti et al., "Hierarchical stochastic neighbor embedding," Computer Graphics Forum 35(3), 2016.

[21] D. Kobak and G. C. Linderman, “UMAP does not preserve global structure any better than t-SNE when using the same initialization,” Preprint: DOI: https://doi.org/10.1101/2019.12.19.877522, 2019.

[22] J. Xie et al., “Unsupervised deep embedding for clustering analysis,” CoRR, abs/1511.06335, 2015.

[23] S. Santurkar et al. “How does batch normalization help optimization?” in Neural Information Processing Systems, 2018.

[24] D. Kingma and J. Ba, “Adam: A method for stochastic optimization,” in International Conference on Learning Representations, 2015. pp. 1-41.

[25] J. Yosinski et al., “Understanding neural networks through deep visualization,” In: ICML Deep Learning Workshop, 2015.

[26] K. Simonyan et al., “Deep inside convolutional networks: visualising image classification models and saliency maps,” In: ICLR Workshop, 2014.

[27] A. T. Elthakeb et al., “Divide and Conquer: Leveraging Intermediate Feature Representations for Quantized Training of Neural Networks,” Preprint: arXiv:1906.06033, 2020.

[28] J. Johnson et al., “Perceptual losses for real-time style transfer and super-resolution,” In: ECCV, 2016.

[29] Y. LeCun et al., “Gradient-based learning applied to document recognition,” In Proceedings of the IEEE, pp. 2278–2324, 1998.

[30] H. Xiao et al., “Fashion-MNIST: a novel image dataset for benchmarking machine learning algorithms,” ArXiv preprints, 2017.

[31] B. Tasic et al., “Shared and distinct transcriptomic cell types across neocortical areas,” Nature, vol. 563, pp. 72–78, 2018.

[32] L. Andrew et al., “Learning word vectors for sentiment analysis,” in Annual Meeting of the Association for Computational Linguistics: Human Language Technologies, pp. 142-150, 2011.

[33] P. Simard et al., “Tangent prop - A formalism for specifying selected invariances in an adaptive network,” in Neural Information Processing Systems, pp. 895–903. 1992.

[34] M. Abadi et al., “TensorFlow: a system for large-scale machine learning,” in Conference on Operating Systems Design and Implementation, Savannah, GA, USA, Nov. 2-4, 2016, pp. 265-283.

[35] M. Espadoto et al., “Towards a quantitative survey of dimension reduction techniques,” IEEE Transactions on Visualization and Computer Graphics, early access, 2019.

[36] L. Nonato and M. Aupetit, “Multidimensional projection for visual analytics: Linking techniques with distortions, tasks, and layout enrichment,” IEEE Transactions on Visualization and Computer Graphics, vol. 25, no. 8, pp. 2650-2673, 2019.

[37] G. Poličar Pavlin et al., “openTSNE: a modular Python library for t-SNE dimensionality reduction and embedding,” bioRxiv, 2019. DOI: 10.1101/731877.

[38] J. Venna and S. Kaski, “Visualizing gene interaction graphs with local multidimensional scaling,” in European Symposium on Artificial Neural Networks, pp. 557–562, 2006.

[39] W. Liu et al., “A survey of deep neural network architectures and their applications,” Neurocomputing, vol. 234, pp. 11-26, 2017.